Adequacy of the Single-Generator Equivalent Model for Stability Analysis in Wind Farms with VSC-HVDC Systems

Shao, Bingbing; Zhao, Shuqiang; Gao, Benfeng; Yang, Y.; Blaabjerg, Frede

Published in:
I E E E Transactions on Energy Conversion

DOI (link to publication from Publisher):
10.1109/TEC.2020.3028546

Publication date:
2021

Document Version
Accepted author manuscript, peer reviewed version

Adequacy of the Single-Generator Equivalent Model for Stability Analysis in Wind Farms with VSC-HVDC Systems

Bingbing Shao, *Student Member, IEEE*, Shuqiang Zhao, Benfeng Gao, Yongheng Yang, *Senior Member, IEEE*, and Frede Blaabjerg, *Fellow, IEEE*

***Abstract*—Due to the complexity of detailed models, the single-generator equivalent model (SEM) of a wind farm is commonly used to facilitate the stability analysis. However, the adequacy of the SEM for stability analysis in direct-drive wind farms with VSC-HVDC systems is still uncertain. Therefore, this paper analyzes the SEM adequacy in two aspects: the oscillation modes analysis and the sub-synchronous oscillation (SSO) stability enhancement by optimizing wind farm parameters. Firstly, various critical oscillation modes are characterized according to the frequency, and a comparison of these modes between the two-generator equivalent model and the SEM is presented. The effect of single-generator aggregation on the critical oscillation modes is discussed. Then, the impact of permanent magnet synchronous generator (PMSG) parameters on the inside-wind-farm/wind-farm-grid SSO modes is explored. It is revealed that with the change of PMSG parameters, the damping effect of the two SSO modes is identical. This implies that the SEM can be used to improve the SSO stability of the multi-machine system by optimizing the PMSG parameters. PSCAD/EMTDC simulations are further performed to verify the theoretical analysis.**

***Index Terms*—Direct-drive permanent magnetic synchronous generator, eigenvalue, equivalent model, stability, sub-synchronous oscillation, VSC-HVDC.**

I. Introduction

DUE to restrictions on land space and wind energy sources, large-scale offshore wind farms are deployed far from the onshore power nodes. When the transmission distance is more than 90 km (common in offshore wind farms), the voltage source converter-based HVDC (VSC-HVDC) technology is more economical for grid connection [1]. As for offshore wind generators, the direct-drive permanent magnet synchronous generator (D-PMSG) is reliable and effective, which does not have gearboxes and any excitation control systems [2]. Thus, the direct-drive wind farm with the VSC-HVDC (DDWFV) is a promising wind energy solution.

However, the stability of the offshore wind farm with VSC-HVDC is a key issue since there is no direct connection from the AC collection bus to a strong AC grid [3]. To investigate the instability in wind farms with VSC-HVDC connections [4], [5], a detailed dynamic model should be built. However, a wind farm model may be comprised of tens or even hundreds of wind turbine generators (WTGs), which significantly enlarges the size of the model and affects the modeling efficiency. Equivalent reduced-order wind farm models have thus been proposed in many power-system studies to enable a fast but accurate assessment of the wind farm performance and the impact on the power grid [6]. The wind farm equivalent models can be obtained using an aggregation method [7], linear/nonlinear model order reduction techniques [8]-[10], [11], equivalent state variables transformation [12], and similarity transformation theory [13]. Compared with the other methods, the aggregation method was widely used in wind farms equivalence because of its clear physical meanings and possibility of physical modeling. The aggregated model can be further divided into the single-generator equivalent model (SEM) and multi-generator equivalent model (MEM). Compared with the MEM, the SEM requires a small amount of calculations and is even better in certain scenarios [14]. With this, instead of proposing a novel equivalent method, the focus of this paper will be on the small-signal stability assessment of the SEM in the DDWFV. To facilitate the following discussion, the inside-wind-farm oscillation modes are defined as the oscillation modes affected by PMSGs rather than by the VSC-HVDC through the participation factors analysis. The wind-farm-grid oscillation modes are defined as the oscillation modes affected by PMSGs and VSC-HVDC systems through the participation factors analysis.

At present, to analyze the small-signal stability of the DDWFV, the SEM is commonly used [15]-[19], but the adequacy of the SEM for stability analysis in the DDWFV has not been discussed yet. As a method to represent the wind farm by a single WTG, the capacity-weighted mean value method has been widely used in engineering practice, but the accuracy of this method is questionable [20]-[22]. A drawback of the SEM lies in that the dynamic characteristics within wind farms may be hidden or the dynamic characteristics of certain critical oscillation modes may be misrepresented [23], [24]. When a wind farm is integrated into an AC network, the SEM has been used in many cases to represent the general dynamic behavior of the wind farm at the point of common coupling (PCC) [25]-[27]. However, the dynamic behavior at the PCC cannot represent the dynamic characteristics inside the wind farm, especially the internal interactive dynamics among WTGs [28]. Thus, an exhaustive stability comparison between the detailed

This work was supported in part by the Natural Science Foundation of Hebei Province under Grant E2017502075, in part by the Fundamental Research Funds for the Central Universities of China under Grant 2018ZD001, and in part by the Joint Postgraduate Training Program of North China Electric Power University.

B. Shao, S. Zhao, and B. Gao are with the Key Laboratory of Distributed Energy Storage and Microgrid of Hebei Province (North China Electric Power University), Baoding 071003, Hebei Province, China (e-mail: shaobingbing1223@163.com; zsqdl@163.com; gaobenfeng@126.com).

Y. Yang and F. Blaabjerg are with the Department of Energy Technology, Aalborg University, Aalborg 9220, Denmark (e-mail: yoy@et.aau.dk; fbl@et.aau.dk).

model and the SEM should be performed, and then, the adequacy of the SEM for the small-signal stability analysis can be explored.

Different aggregated models have been compared in the literature. In [6], the SEM, the semi aggregated model, and the MEM were compared by simulations at the PCC. Based on the aggregation criterion, three aggregated PMSG wind farm models were compared by simulations at the PCC [7]. In [14], an exhaustive simulation at the PCC was presented to validate the adequacy of the SEM and the MEM, and it was concluded that we cannot take it for granted that an MEM performs better than an SEM. By incorporating the nonlinear wake model and frequency-regulation function, a multi-machine doubly fed induction generator (DFIG) equivalent method was proposed in [29] and compared with the SEM. Considering the DFIGs' low voltage ride-through (LVRT) behaviors, the "error and impact" of an aggregation-based representation of wind farms was analyzed in [20], [30]. It was concluded in [20] that the equivalent error of the SEM mainly resulted from the active power recovery stage during the fault-ride-through (FRT) process. In [31], a dynamic simulation comparison between the single- and multiple-turbine representation was presented in a wind farm. It can be found in [6], [7], [14], [20], [29]-[31] that the comparisons between various aggregated models and the validations of improved aggregated models were performed by simulations at the PCC. However, time-domain simulations cannot clearly reveal all oscillation modes and their manifestations. Thus, the simulations cannot be used to evaluate the effectiveness of the equivalent models in small-signal stability analysis, and then guidelines for future equivalence cannot be proposed properly [32]. Moreover, the simulations at the PCC cannot reflect the dynamic interactions among WTGs.

In light of this, the small-signal stability analysis was performed to evaluate the wind farm equivalent models [12], [13], [24], [32]-[39]. To estimate the equivalent parameters of DFIG wind farms, an aggregation technique consisting of a hybrid algorithm was proposed by using the measurement data from phasor measurement units (PMUs) [33]. The PMU was also applied in [34], [35] to identify the equivalent parameters of hybrid WTGs. The improved aggregated models in [33]-[35] were evaluated by modal comparisons with the detailed model. Based on the impedance analysis method, the DFIG and PMSG models were simplified into impedance models, and then aggregated impedance models were proposed to investigate the sub-synchronous oscillation (SSO) of wind farms [36], [37], where the impedance characteristics analysis was performed to evaluate the aggregated impedance models. To facilitate the small-signal stability analysis of wind farms, three equivalent methods were proposed by modal participation factor aggregation criterion [32], equivalent state variables transformation [12], and similarity transformation theory [13]. To investigate the impact of the SEM on the critical modes under weak grid conditions compared to the MEM, a small-signal based benchmarking between the two equivalent models was presented in [24]. In [38], [39], the oscillation modes comparisons between the detailed model and the SEM in the case of a large number of grid-connected inverters were presented.

Although there is an adequacy study on the equivalent models for small-signal stability analysis in wind farms directly connected to an AC grid [12], [13], [24], [32]-[37] and grid-connected inverters [38], [39], the accuracy of the SEM has not been studied in the case of the DDWFV. Different from the wind farms directly connected to the AC grid, the oscillation interactions between the grid-side converter (GSC) of the PMSG and the rectifier (REC) of the VSC-HVDC exist in the DDWFV [3]. Although the adequacy of the MEM for the oscillation modes analysis was explored in wind farms with VSC-HVDC systems [23], [40], the converter dynamics of the VSC-HVDC were neglected and represented only by an impedance, and the adequacy of the SEM was not discussed. On the other hand, the adequacy of the SEM for improving the SSO stability by optimizing PMSG parameters is still unclear. As there are inside-wind-farm and wind-farm-grid SSO modes in the DDWFV [23], [41], there is a damping coupling relationship between the two oscillation modes with the change of PMSG parameters. Thus, while using the SEM to improve the SSO stability by adjusting PMSG parameters, the inside-wind-farm SSO damping in practical multi-generator models also changes. When the damping trends of inside-wind-farm and wind-farm-grid SSO modes are not identical, the inside-wind-farm SSO damping will decrease and practical multi-generator models will become risky of instability due to the tuning of PMSG parameters. Although the inside-wind-farm SSO modes have been detected in the DDWFV [23], the impact of system parameters on the SSO interaction modes was not analyzed.

In brief, through the above analysis, three gaps exist in the SEM studies of the DDWFV: a) the adequacy of the SEM for oscillation modes analysis has not been analyzed, b) the impact of PMSG parameters on inside-wind-farm SSO modes has not been analyzed, c) the adequacy of the SEM for improving the SSO stability by optimizing PMSG parameters has not been explored, neither in the DDWFV nor in the direct-drive wind farms directly connected to the AC grid.

To fill in the three gaps in this paper, the adequacy of the SEM for stability analysis in the DDWFV is analyzed in two aspects: the oscillation modes analysis and the SSO stability enhancement by optimizing the PMSG parameters. Meanwhile, the inside-wind-farm SSO characteristics are investigated in the process of the adequacy analysis. Aiming at a), various oscillation modes are classified according to the frequency. A comparison of critical oscillation modes between the two-generator equivalent model (TEM) and the SEM is presented, and the impact of the SEM on the oscillation modes analysis is discussed. To fill in the gap b), the impact of PMSG parameters on the inside-wind-farm SSO characteristics is analyzed by the eigenvalue analysis. Regarding c), the damping coupling characteristics between the inside-wind-farm SSO modes and wind-farm-grid SSO modes are explored, and then the adequacy of the SEM for improving the SSO stability by optimizing PMSG parameters is explored.

The rest of this paper is organized as follows. In Section II, the small-signal model of the DDWFV is built. Subsequently, the comparison of the critical oscillation modes between the TEM and the SEM is presented in Section III, where the adequacy of the SEM for oscillation modes analysis is discussed. By exploring the damping coupling characteristics between inside-wind-farm SSO modes and wind-farm-grid

This article has been accepted for publication in a future issue of this journal, but has not been fully edited. Content may change prior to final publication. Citation information: DOI 10.1109/TEC.2020.3028546, IEEE Transactions on Energy Conversion

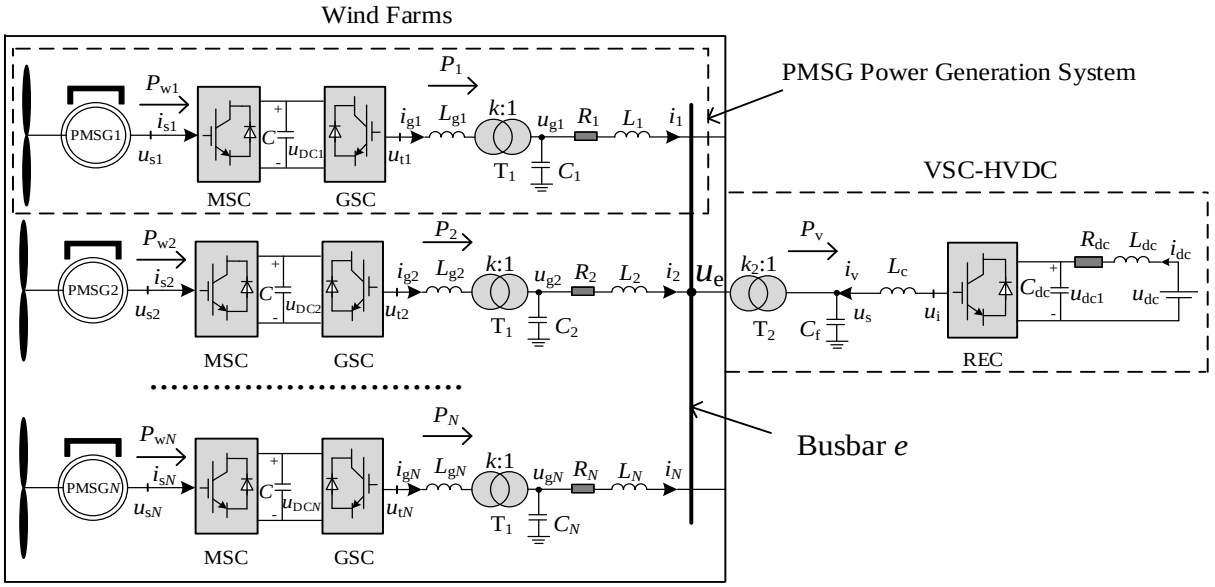

Fig. 1. Configuration of a direct-drive wind farm with VSC-HVDC systems: MSC - machine-side converter, GSC - grid-side converter, REC - rectifier.

SSO modes, the adequacy for improving the SSO stability by optimizing PMSG parameters is analyzed in Section IV. Concluding remarks are given in Section V.

II. Modeling of the DDWFV

The structure of a multi-PMSG based wind farm with the VSC-HVDC is shown in Fig. 1. The system is divided into two parts: wind farms and VSC-HVDC system. The wind farms include several PMSG power generation systems. After the back-to-back conversion, the voltage is converted to 35 kV by the machine-side step-up transformer T_1, and then transferred to the busbar *e* through submarine AC transmission cables. Finally, the AC voltage is converted to 110 kV by an offshore step-up transformer T_2, and then, the wind power is delivered to the VSC-HVDC system. The machine-side converter (MSC) adopts the space vector control strategy based on the rotor flux linkage, and the GSC utilizes the space vector control strategy based on the grid voltage.

A. Dynamic Model of Wind Farms

A complete dynamic model of the PMSG wind farm includes the drive train, PMSG, back-to-back converter, phase-locked loop (PLL), and collector lines. The derivation of these dynamic models has been well documented in [28], [42] and will not be discussed here. The MSC controls the *d*-axis current to be 0, which minimizes the loss in the generator. The DC voltage and reactive power are controlled by the GSC. The PLL control structure of the PMSG adopts the structure in [28]. The control of the back-to-back converter uses the method in [43]. The system and control parameters of the single PMSG power generation system are the same as those in [43], where the bandwidths of the PLL, outer loop DC voltage control and inner loop current control are 3 Hz, 45 Hz and 477 Hz, respectively. The wind speed is set to 8 m/s, and the initial parameters of each PMSG power generation system are identical.

Considering the dynamic modeling of the drive train, PMSG, back-to-back converter, PLL, and wind power collector lines, the state variables of each PMSG power generation system are divided into five groups according to the relevant modules, as shown in Table I, where x_1-x_6, x_a, and x_b are given as

$$\begin{cases} \mathrm{d}x_1/\mathrm{d}t = i_{d\mathrm{sref}} - i_{d\mathrm{s}} \\ \mathrm{d}x_2/\mathrm{d}t = \omega_{\mathrm{sref}} - \omega_{\mathrm{s}} \\ \mathrm{d}x_3/\mathrm{d}t = i_{q\mathrm{sref}} - i_{q\mathrm{s}} \\ \mathrm{d}x_4/\mathrm{d}t = u_{\mathrm{DC}} - u_{\mathrm{DCref}} \\ \mathrm{d}x_5/\mathrm{d}t = i_{d\mathrm{gref}} - i_{d\mathrm{g}} \\ \mathrm{d}x_6/\mathrm{d}t = i_{q\mathrm{gref}} - i_{q\mathrm{g}} \\ \mathrm{d}x_{\mathrm{a}}/\mathrm{d}t = u_{q\mathrm{g}} \\ \mathrm{d}x_{\mathrm{b}}/\mathrm{d}t = \omega_0 + u_{q\mathrm{g}} k_{\mathrm{ppll}} + u_{q\mathrm{g}} T_{\mathrm{ipll}} \end{cases} \tag{1}$$

TABLE I
Grouping of State Variables in Each PMSG Power Generation System

Modules	State variables
Shaft	Wind turbine speed: ω_s
PMSG	Stator current: i_{ds} and i_{qs}
Back-to-back converter	DC voltage: u_{DC} *d*-axis current controller of MSC: x_1 Constant speed controller: x_2 and x_3 Constant DC voltage controller: x_4 and x_5 *q*-axis current controller of GSC: x_6
Grid-connected collector lines	GSC side current: i_{dg} and i_{qg} GSC side voltage: u_{dg} and u_{qg} Collector line current: i_d and i_q
PLL	x_a and x_b

where k_{ppll} and T_{ipll} are the proportional coefficient and integral time constant in the PLL, respectively ($k_{\mathrm{ppll}} = 5$, $T_{\mathrm{ipll}} = 9$). $\omega_0 = 2\pi f_0$ is the reference angular frequency with $f_0 = 50$ Hz. The subscript "ref" implies the reference value of variables, and the subscripts *d* and *q* imply the *d*- and *q*-axis components of variables, respectively. The variables of the single PMSG power generation system include the state variables $\boldsymbol{x}_{wi} = [\omega_{si}, i_{dsi}, i_{qsi}, u_{DCi}, x_{1i}, x_{2i}, x_{3i}, x_{4i}, x_{5i}, x_{6i}, i_{dgi}, i_{qgi}, u_{dgi}, u_{qgi}, i_{di}, i_{qi}, x_{ai}, x_{bi}]$, the input variables $\boldsymbol{u}_{wi} = [i_{d\mathrm{srefi}}, \omega_{\mathrm{srefi}}, u_{\mathrm{DCrefi}}, i_{q\mathrm{srefi}}]$, and *i* represents the *i*-th PMSG power generation system. Therefore, each PMSG power generation system contains 18 state variables and 4 input variables.

B. Dynamic Model of the VSC-HVDC

In Fig. 1, the REC controls the amplitude and frequency of u_s, and the inverter controls the DC voltage. Supposing that the onshore AC grid is strong, the DC bus voltage can be kept constant by the inverter station, and then, a constant DC voltage source is applied to be equivalent to the function of the inverter station, shown as u_{dc} in Fig. 1 [15]. A complete dynamic model of the VSC-HVDC includes the AC system network, DC system network, REC controller, and PLL controller, which have been well discussed in [44]. The control structure of the REC adopts the structure in [43], and the PLL of the VSC-HVDC takes the reference angular frequency ω_0 as the input signal, and thus, there is no state variable in the PLL of the VSC-HVDC [3]. The parameters of the VSC-HVDC are the same as those in [43], where the bandwidth of the inner loop current control is 203 Hz.

Considering the dynamic modeling of the AC system, DC system, and REC, the state variables of the VSC-HVDC system are obtained. They are divided into three groups according to the relevant modules, as shown in Table II, where x_7 and x_8 are given as

$$\begin{cases} \mathrm{d}x_7 / \mathrm{d}t = i_{d\mathrm{vref}} - i_{dv} \\ \mathrm{d}x_8 / \mathrm{d}t = i_{q\mathrm{vref}} - i_{qv} \end{cases} \tag{2}$$

The state variables of the VSC-HVDC system are $\boldsymbol{x}_v = [u_{ds}, u_{qs}, i_{dv}, i_{qv}, i_{dc}, u_{dc1}, x_7, x_8]$, and the input variables are $\boldsymbol{u}_v = [u_{ds\mathrm{ref}}, u_{qs\mathrm{ref}}]$. Therefore, the VSC-HVDC contains 8 state variables and 2 input variables.

TABLE II
GROUPING OF STATE VARIABLES IN THE VSC-HVDC

Modules	State variables
AC system	AC voltage: u_{ds} and u_{qs} AC current: i_{dv} and i_{qv}
DC system	DC current and DC voltage: i_{dc} and u_{dc1}
REC	Inner loop of *d*-axis voltage controller: x_7 Inner loop of *q*-axis voltage controller: x_8

C. Small-Signal Model

According to the dynamic modeling of the above subsystems, the complete dynamic mathematical model of the DDWFV can be obtained. The process of modeling, linearization, and eigenvalues solution using MATLAB/Simulink is directed to [23]. After linearization, the small-signal model is expressed as

$$\frac{\mathrm{d}\Delta \boldsymbol{x}}{\mathrm{d}t} = \boldsymbol{A}\Delta \boldsymbol{x} + \boldsymbol{B}\Delta \boldsymbol{u} \tag{3}$$

where $\Delta\boldsymbol{x}$ is the linearized state variable, $\Delta\boldsymbol{u}$ is the linearized input variable, $\boldsymbol{A}$ is the state matrix, and $\boldsymbol{B}$ is the input matrix. For an N-machine with the VSC-HVDC system, the state variables are $\boldsymbol{x}_N = [\boldsymbol{x}_{w1}, \boldsymbol{x}_{w2}, \ldots, \boldsymbol{x}_{wN}, \boldsymbol{x}_v]^T$, and the input variables are $\boldsymbol{u}_N = [\boldsymbol{u}_{w1}, \boldsymbol{u}_{w2}, \ldots, \boldsymbol{u}_{wN}, \boldsymbol{u}_v]^T$.

III. ADEQUACY FOR OSCILLATION MODES ANALYSIS

A. Equivalent Principle

Referring to the equivalent principle of [45], each wind farm is assumed to have 40 turbines with 2.5 MW capacity for each. To simplify the system model, 40 turbines are lumped into one unit of 100 MW PMSG power generation capacity, as shown in Fig. 1. The equivalent PMSG power generation system consists of a generator, a transformer, and an impedance. The following assumptions to derive the aggregated model are made:

1) Currents in the collector system shunt admittances are negligible.
2) Reactive power generated by line shunt capacitors is based on the assumption that the voltage at the buses is one per unit.

The aggregation of WTGs, transformers, and collector cables are performed as follows:

1) Aggregation of WTGs: The capacity of the equivalent machine is equal to the sum of the capacities of the generators aggregated. The electrical and mechanical parameters of the aggregated machine in per unit are the same as the WTG in respective machine base. The equivalent wind speed is obtained from an equivalent power curve as [46]

$$v_{\mathrm{eq}} = f^{-1}\left(\frac{1}{N}\sum_{m=1}^{N} f(v_m)\right) \tag{4}$$

where f is the power-wind speed curve, N is the number of the WTGs aggregated, and v_{eq} is the equivalent wind speed.

2) Aggregation of the transformers and collector cables: The capacity of the equivalent transformer is equal to the sum of the capacities of the transformers aggregated. For wind farms in parallel, the equivalence process of the transformers and collector cables is shown in Fig. 2.

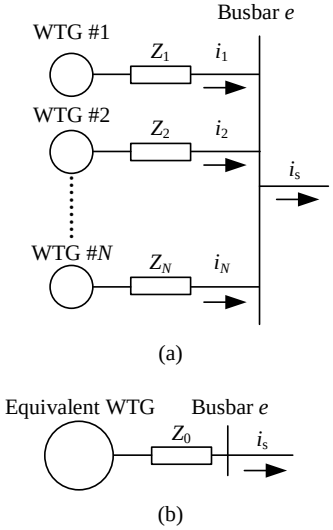

Fig. 2. Equivalent process of transformers and collector cables: (a) N WTGs in parallel connection and (b) Equivalent circuit.

Fig. 2(a) shows N WTGs in parallel, and Z_m (m = 1, 2, …, N) denotes the impedance of transformers or collector cables in m-th WTG. As each WTG is controlled to have a unity power factor, the apparent power S_m in the m-th WTG can be substituted by the rated active power P_m of the m-th WTG. The voltage drop ΔV_m across Z_m is written as

$$\Delta V_m = i_m Z_m = (S_m / V) Z_m = P_m Z_m / V \tag{5}$$

where V is the voltage at the buses. Then, the apparent power loss across Z_m is derived as

$$\Delta S_m = \Delta V_m i_m^* = (P_m Z_m / V)(P_m / V)^* = P_m^2 Z_m / V^2 \tag{6}$$

Fig. 2(b) shows the equivalent circuit to represent the aggregated transformers or collector cables, and Z_0 is the equivalent impedance. The voltage drop ΔV_0 and apparent

This article has been accepted for publication in a future issue of this journal, but has not been fully edited. Content may change prior to final publication. Citation information: DOI 10.1109/TEC.2020.3028546, IEEE Transactions on Energy Conversion

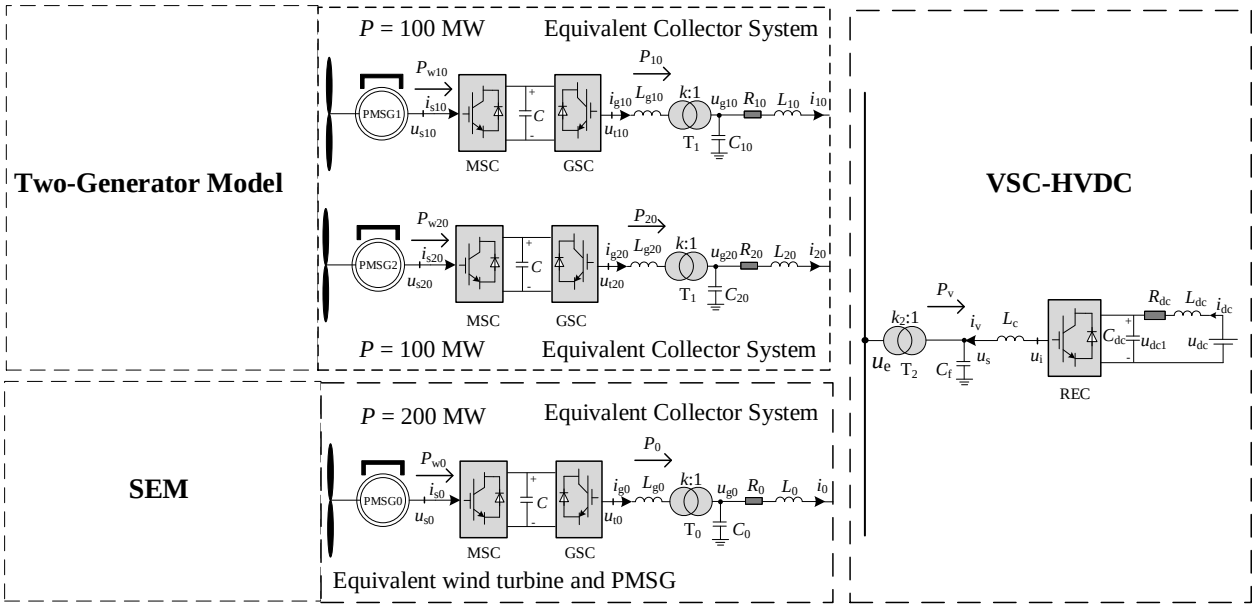

Fig. 3. Two-generator equivalent model (TEM) and the single-generator equivalent model (SEM) of the direct-drive wind farms with the VSC-HVDC.

power loss ΔS_0 across Z_0 are derived as

$$\Delta V_0 = i_s Z_0 = \sum_{m=1}^{N} P_m Z_0 / V \tag{7}$$

$$\Delta S_0 = \Delta V_0 i_s^* = (\sum_{m=1}^{N} P_m Z_0 / V)(\sum_{m=1}^{N} P_m / V)^* = (\sum_{m=1}^{N} P_m)^2 Z_0 / V^2 \tag{8}$$

Based on the principle that the apparent power losses in the equivalent impedance are equal to the apparent power losses in the impedances aggregated, by combining (6) and (8), the expression of the equivalent impedance is written as

$$Z_0 = \frac{\sum_{m=1}^{N} P_m^2 Z_m}{(\sum_{m=1}^{N} P_m)^2} \tag{9}$$

Meanwhile, considering that the bus voltage is close to unity under normal conditions, the shunt admittance of the equivalent collector cable is equal to the sum of all the admittances in the wind farm collector networks as

$$B_0 = \sum_{m=1}^{N} B_m \tag{10}$$

where B_0 is the equivalent shunt admittance of the collector cable, and B_m (m = 1, 2, …, N) denotes the shunt admittance of the collector cable in m-th WTG.

The other equivalent system parameters and control parameters remain unchanged. Based on the above equivalent principle, the adequacy of the SEM for oscillation modes analysis will be discussed by comparing the following models:

1) The TEM: The multi-machine model is normally grouped based on the coherency criterion, e.g., wind speed, wind direction, and layout of wind farms [38]. Assuming that every 40 WTGs present similar dynamic characteristics, the multi-machine model of the wind farm can be divided into two models, each with 100 MW (40 × 2.5 MW) capacity. Such two-machine aggregation can also refer to [24], [47]. In this case, the whole wind farm is modelled by two equivalent WTGs with 100 MW capacity for each, as shown in Fig. 3.

2) The SEM: The full aggregated model of a large wind farm with 200 MW (80 × 2.5 MW) capacity. In this case, the whole wind farm is lumped into one equivalent WTG with 200 MW rated power, as shown in Fig. 3. It is worth pointing out that the SEM can be regarded as the further aggregated model of the TEM, whereas the TEM is regarded as the detailed model in such case [45]. Thus, applying the TEM to imitate the detailed model for oscillation modes comparison with the SEM is reasonable.

B. Modes Comparison Between the SEM and the TEM

The critical oscillation modes are analyzed under the SEM and the TEM by the eigenvalue analysis, as listed in Tables III and IV. To facilitate the oscillation modes comparison between the SEM and the TEM, the SSO mode, medium-frequency mode and high-frequency mode are defined [41].

TABLE III
OSCILLATION MODES UNDER THE SEM

Oscillation modes	Eigenvalues	Oscillation frequency (Hz)	Damping ratio
A1	12.973±j102.64	16.34	-0.1254
A2	446.90±j1543.0	245.58	-0.2781
A3	-31.768±j3651.4	581.14	0.0087
A4	-569.01±j1257.7	200.17	0.4122
A5	-92.817±j796.14	126.71	0.1158
A6	-17.109±j2851.5	453.83	0.0060

TABLE IV
OSCILLATION MODES UNDER THE TEM

Oscillation modes	Eigenvalues	Oscillation frequency (Hz)	Damping ratio
F1	11.983±j104.15	16.58	-0.1143
F2	8.5598±j105.46	16.78	-0.0809
F3	-31.768±j3651.4	581.14	0.0087
F4	-214.60±j1327.4	211.26	0.1596
F5	-88.761±j774.91	123.33	0.1138

1) SSO Mode: Modes having frequencies in the range of 2.5 Hz to 50 Hz. There is one SSO mode (A1) in the SEM and two SSO modes (F1 and F2) in the TEM.

2) Medium-Frequency Mode (MFM): Modes having

frequencies in the range of 50-500 Hz. There are four MFMs (A2, A4, A5, and A6) in the SEM and two MFMs (F4 and F5) in the TEM.

3) High-Frequency Mode (HFM): Modes having frequencies in the range of 500 Hz to 2 kHz. There is one HFM (A3) in the SEM and one HFM (F3) in the TEM.

To obtain the state variables that affect these oscillation modes in the SEM and the TEM, the main participating state variables and corresponding normalized participation factors of these modes are calculated, as shown in Table V, where the participating state variables with low participation factors are not listed. To facilitate the subsequent analysis without loss of generality, the oscillation modes with similar participating state variables and participation factors are considered to be the same type of oscillation modes, and the other modes are considered as the extra modes.

C. Analysis of SSO Modes

It is noticeable that both models have the same type of unstable SSO modes (A1 and F1). The frequency and damping ratio of the two SSO modes are almost identical. It can be seen from Table V that the two SSO modes are mainly influenced by u_{DC}, x_4, x_5, i_{dg} in PMSGs and u_{ds}, i_{dv}, x_7 in the VSC-HVDC. Therefore, A1 and F1 are not only affected by the DC voltage controllers of PMSGs, but also affected by the *d*-axis voltage controller of the VSC-HVDC. That is, the two SSO modes are wind-farm-grid SSO_2 modes.

Compared with the SEM, the TEM has one more SSO mode F2, and F2 shows negative damping of the system. F2 is mainly influenced by u_{DC}, x_4, x_5, i_{dg} in PMSGs, and not affected by the VSC-HVDC. Thus, F2 is an inside-wind-farm SSO_1 mode which is affected by the DC voltage controllers of PMSGs. The SEM can reflect the wind-farm-grid SSO_2 modes, but it hides the inside-wind-farm SSO_1 modes because it does not consider the interactions among multiple PMSGs in wind farms.

D. Analysis of MFMs

As it can be seen from Table V, A4 and A5 in the SEM correspond to F4 and F5 in the TEM, respectively. They have main participation from the VSC-HVDC part and minor participation from the wind farm. It should be noted that although they have similar oscillation frequencies, there is a significant difference between the damping ratios of A4 and F4.

Compared with the TEM, the SEM has two more MFMs, i.e., A2 and A6. A2 is negatively damped to the system, and A6 shows weak damping to the system. It can be seen from Table V that A2 and A6 are related to the state variables of the wind farm and the VSC-HVDC, which means that they are wind-farm-grid oscillation modes. In addition, the participation of the wind farm in A2 and A6 is larger than that of the VSC-HVDC. These modes are the result of equivalencing cable parameters and representing them as lumped elements. Considering the inertia of the SEM to represent a two-generator model, the SEM has two times higher inertia compared with one generator in the TEM, which moves certain HFMs in the TEM to the range of the MFMs [40]. This explains why certain additional MFMs appear in the SEM.

E. Analysis of HFMs

As it can be seen from Table V, HFMs, i.e., A3 and F3, have the same participating state variables and normalized participation factors from the DC system of the VSC-HVDC. As the modeling of the VSC-HVDC subsystem remains unchanged in the SEM and the TEM, the oscillation frequencies and damping ratios of A3 and F3 are identical.

F. Simulation Results

1) SEM Simulation Verification: In order to verify the eigenvalue analysis in Table III under the SEM, a simulation model of the SEM referring to Fig. 3 is built in PSCAD/EMTDC. The parameters of the initial detailed model are given in [43]. It was revealed in [48] that the discrepancies

TABLE V
PARTICIPATING STATE VARIABLES AND CORRESPONDING NORMALIZED PARTICIPATION FACTORS OF THE SEM AND THE TEM

SEM		TEM	
Corresponding modes	Participating state variables and corresponding normalized participation factors in bracket	Corresponding modes	Participating state variables and corresponding normalized participation factors in bracket
SSO mode A1	Equivalent PMSG (0.8451): u_{DC} (0.3808), x_4 (0.3687), x_5 (0.0048), i_{dg} (0.0908) VSC-HVDC (0.1471): u_{ds} (0.0465), i_{dv} (0.0447), x_7 (0.0559)	SSO mode F1	1st PMSG (0.4602)/2nd PMSG (0.4602): $u_{DC1,2}$ (0.2033), $x_{41,42}$ (0.1973), $x_{51,52}$ (0.0026), $i_{dg1,2}$ (0.0570) VSC-HVDC (0.0793): u_{ds} (0.0251), i_{dv} (0.0242), x_7 (0.0300)
MFM A4	Equivalent PMSG (0.4305): u_{dg} (0.3281), u_{qg} (0.0136), i_d (0.0839), i_q (0.0049) VSC-HVDC (0.5673): u_{ds} (0.2760), u_{qs} (0.0162), i_{dv} (0.1253), i_{qv} (0.0074), x_7 (0.1345), x_8 (0.0079)	MFM F4	1st PMSG (0.1459)/2nd PMSG (0.1459): $u_{dg1,2}$ (0.1112), $u_{qg1,2}$ (0.0046), $i_{d1,2}$ (0.0284), $i_{q1,2}$ (0.0017) VSC-HVDC (0.7058): u_{ds} (0.3070), u_{qs} (0.0169), i_{dv} (0.1819), i_{qv} (0.0100), x_7 (0.1801), x_8 (0.0099)
MFM A5	Equivalent PMSG (0.0553): u_{dg} (0.0280), u_{qg} (0.0122), i_d (0.0082), i_q (0.0069) VSC-HVDC (0.9435): u_{ds} (0.0015), u_{qs} (0.0280), i_{dv} (0.0226), i_{qv} (0.4351), x_7 (0.0225), x_8 (0.4338)	MFM F5	1st PMSG (0.015)/2nd PMSG (0.015): $u_{dg1,2}$ (0.0076), $u_{qg1,2}$ (0.0033), $i_{d1,2}$ (0.0022), $i_{q1,2}$ (0.0019) VSC-HVDC (0.9687): u_{ds} (0.0057), u_{qs} (0.0419), i_{dv} (0.0555), i_{qv} (0.4057), x_7 (0.0554), x_8 (0.4045)
HFM A3	VSC-HVDC (1.0000): i_{dc} (0.5000), u_{dc1} (0.5000)	HFM F3	VSC-HVDC (1.0000): i_{dc} (0.5000), u_{dc1} (0.5000)
Extra modes		Extra modes	
MFM A2	Equivalent PMSG (0.5206): u_{dg} (0.3676), u_{qg} (0.0154), i_d (0.1280), i_q (0.0096) VSC-HVDC (0.4779): u_{ds} (0.2752), u_{qs} (0.0144), i_{dv} (0.0962), i_{qv} (0.0050), x_7 (0.0828), x_8 (0.0043)	SSO mode F2	1st PMSG (0.5000)/2nd PMSG (0.0005): $u_{DC1,2}$ (0.2198), $x_{41,42}$ (0.2145), $x_{51,52}$ (0.0028), $i_{dg1,2}$ (0.0629)
MFM A6	Equivalent PMSG (0.9532): u_{dg} (0.0548), u_{qg} (0.4408), i_d (0.0271), i_q (0.4305) VSC-HVDC (0.0459): u_{ds} (0.0283), u_{qs} (0.0108), i_{dv} (0.0031), i_{qv} (0.0012), x_7 (0.0025)		

This article has been accepted for publication in a future issue of this journal, but has not been fully edited. Content may change prior to final publication. Citation information: DOI 10.1109/TEC.2020.3028546, IEEE Transactions on Energy Conversion

between the simulation results and the actual results resulted from the wind variations, but such condition does not exist in this paper. The equivalent parameters of WTGs, transformers, and collector cables are set based on the equivalent principle in Section III-A. It can be seen from Table III that there are four weakly damped or unstable oscillation modes (SSO mode A1, MFMs A2 and A6, HFM A3). These modes play an important role in the system stability and should be verified, whereas the other modes in Table III decay fast and have a negligible impact on the system stability. The outer loop integral coefficient (k_{i4}) of the DC voltage controller is changed from 20 to 400 at 1.3 s. The waveforms and spectrum analysis of the *d*-axis and *q*-axis voltage at the PCC are shown in Figs. 4 and 5.

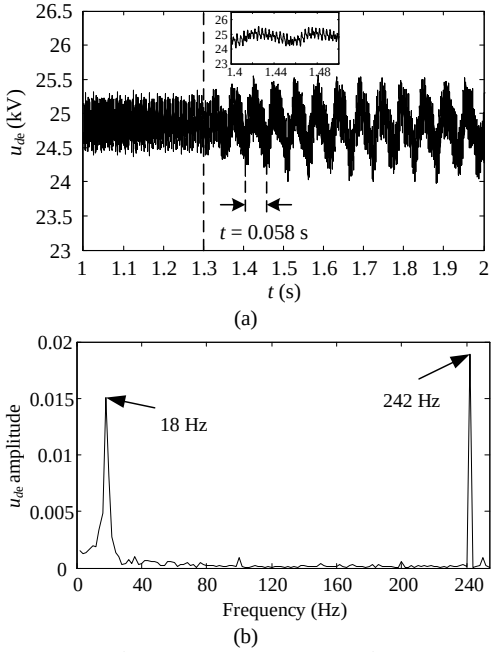

Fig. 4. Simulation waveform and spectrum analysis of the *d*-axis voltage at the PCC following a change of k_{i4} from 20 to 400 in the single-generator equivalent model: (a) simulation waveform and (b) spectrum analysis.

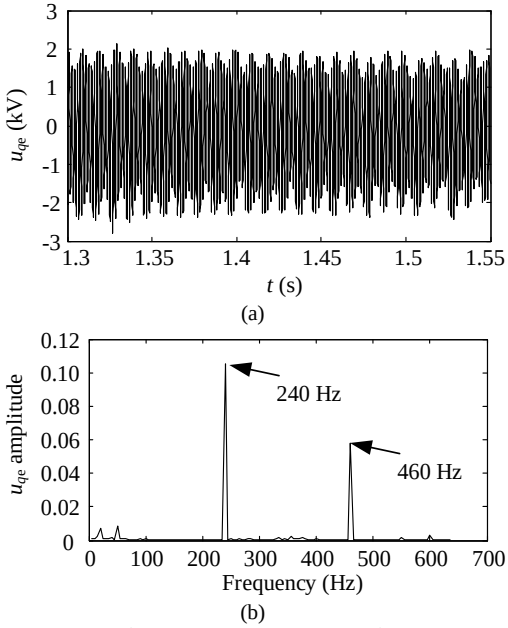

Fig. 5. Simulation waveform and spectrum analysis of the *q*-axis voltage at the PCC following a change of k_{i4} from 20 to 400 in the single-generator equivalent model: (a) simulation waveform and (b) spectrum analysis.

It can be seen from Fig. 4 that u_{de} mainly contains an unstable SSO component of 17.24 Hz (the oscillation period is 0.058 s) and a medium-frequency oscillation component of 242 Hz (see the zoom-in view of Fig. 4(a)). Meanwhile, it can be known from Table III that the two oscillation frequencies correspond to the frequencies of unstable oscillation modes, A1 and A2. It can be seen from Fig. 5 that u_{qe} mainly contains two oscillation components, and their frequencies are 240 Hz and 460 Hz, which correspond to the frequencies of A2 and A6 in Table III.

To verify the HFM A3, the simulation waveform of the DC voltage (u_{dc1} with 160 kV rated voltage) at the VSC-HVDC is shown in Fig. 6. Fig. 6 shows that u_{dc1} contains an HFM component about 588 Hz (the oscillation period is 0.0017 s). This component corresponds to the HFM A3 in Table III.

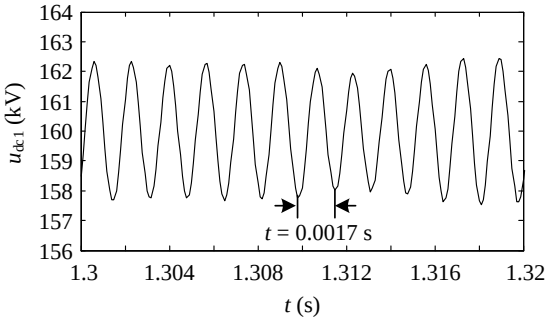

Fig. 6. Simulation waveform of the DC voltage (u_{dc1}) at the VSC-HVDC in the single-generator equivalent model.

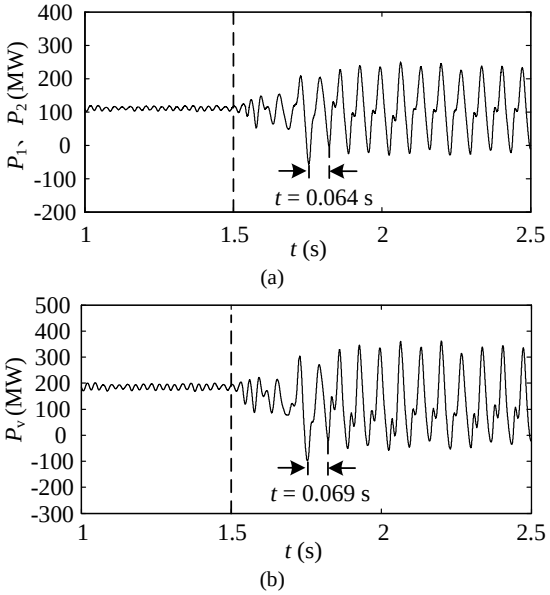

Fig. 7. Simulation results when k_{i4} changes from 20 to 400 in the two-generator model: (a) output active power P_1, P_2 of PMSGs and (b) output active power P_v of the VSC-HVDC.

2) TEM Simulation Verification: In order to verify the eigenvalue analysis in Table IV under the TEM, a simulation model of a two-generator PMSG-based wind farm with the VSC-HVDC is built in PSCAD/EMTDC according to Fig. 3, and k_{i4} is changed from 20 to 400 at 1.5 s. The inside-wind-farm SSO_1 mode F2 should be observed in the wind farm, and the wind-farm-grid SSO_2 mode F1 should be observed in the VSC-HVDC. Therefore, the waveforms of the output active power P_1, P_2 in the grid side of the first and second PMSGs and the output active power P_v in the VSC-HVDC are shown in Fig. 7. It can be seen from Fig. 7(a) that the oscillation frequency of

This article has been accepted for publication in a future issue of this journal, but has not been fully edited. Content may change prior to final publication. Citation information: DOI 10.1109/TEC.2020.3028546, IEEE Transactions on Energy Conversion

the output active power in two PMSGs is 15.63 Hz (the oscillation period is 0.064 s), which is close to the oscillation frequency of the inside-wind-farm SSO_1 mode F2 in Table IV (16.78 Hz). Meanwhile, Fig. 7(b) shows that the oscillation frequency of the output active power of the VSC-HVDC is 14.49 Hz (the oscillation period is 0.069 s), which is close to the oscillation frequency of the wind-farm-grid SSO_2 mode F1 in Table IV (16.58 Hz). Moreover, the inside-wind-farm SSO frequency in Fig. 7(a) is more than the wind-farm-grid SSO frequency in Fig. 7(b), and the same conclusion can be obtained from the eigenvalue analysis in Table IV.

The waveform of the DC voltage (u_{dc1}) at the VSC-HVDC is shown in Fig. 8. It can be observed in Fig. 8 that u_{dc1} contains an HFM component about 588 Hz (the oscillation period is 0.0017 s), which corresponds to the HFM F3 in Table IV.

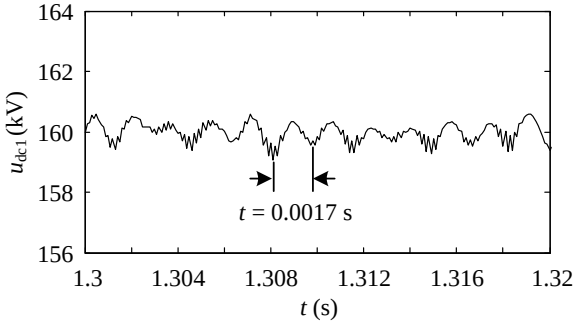

Fig. 8. Simulation waveform of the DC voltage (u_{dc1}) at the VSC-HVDC in the two-generator model.

G. Summary of Oscillation Modes Comparison Between the SEM and the TEM

According to the above analysis, although the SEM preserves the dynamic characteristics of the wind-farm-grid SSO modes and the frequency characteristics of the TEM, there are differences in the number of modes and their damping. Compared with one generator in the TEM, the SEM has two times higher inertia, which moves certain HFMs in the TEM to the range of the MFMs. Therefore, the SEM contains two more wind-farm-grid MFMs (A2 and A6), one of which is negatively damped, and the other is weakly damped. These modes are merely the result of aggregation and will not appear in practice. Meanwhile, as the TEM can reflect the interaction between two WTGs, the TEM contains one more negatively damped inside-wind-farm SSO mode (F2), and this mode is mainly affected by the DC voltage controllers of two PMSGs. In fact, the main reason for the differences between the two models is that the adopted equivalent principle in [45] only focuses on the power flow analysis and the entire response at the PCC, whereas the inner dynamics of the wind farm are not considered as only one WTG is taken into account. Besides, the aggregation of converters is not considered in the principle. However, it can be seen from Table V that many modes are affected by the converter controllers. Therefore, there is a significant difference between the damping ratio of the MFMs, A4 and F4, as shown in Tables III and IV. In brief, there are obvious differences between the SEM and the TEM in their dynamic characteristics. The simple single-generator aggregation of wind farm masks some of the internal oscillation modes (such as the unstable inside-wind-farm SSO mode F2) within the wind farm or alter their characteristics (such as A4 and F4), and certain additional MFMs (such as A2 and A6) may exist because of the aggregation of cable parameters. Some guidelines for the future aggregation in the DDWFV are provided as follows:

1) As there might be certain unstable inside-wind-farm SSO modes in the multi-machine model, the aggregation of wind farm should consider the interactions among WTGs.
2) As certain weakly damped or unstable oscillation modes are affected by control parameters and dynamic characteristics of converters, an aggregated model should be proposed to fit the dynamic characteristics of converters and control systems.

It is worth mentioning that the bandwidth of the PLL and DC voltage controller of the PMSG power generation system is set different in the system under study. When the bandwidth of the PLL is close to the bandwidth of the DC voltage controller, the interaction between the PLL and DC voltage controller will become strong, and then the PLL may participate in the SSO modes to a large extent [49]. In this case, the participation factors analysis in Table V should include the state variables of the PLL, which will be the future work.

IV. Adequacy for the SSO Stability Enhancement by Optimizing PMSG Parameters

Table V shows that the inside-wind-farm SSO mode F2 (defined as the SSO_1 mode in this section) and the wind-farm-grid SSO mode F1 (defined as the SSO_2 mode in this section) are related to the state variables of PMSGs. Thus, there is a damping coupling relationship between the two SSO modes with the change of PMSG parameters. Once the damping trends of the two SSO modes are different, while optimizing PMSG parameters to increase the damping of SSO_2 modes in the SEM, the damping of SSO_1 modes in the TEM is reduced. This may lead to an unstable TEM and has an adverse impact on the system stability. In order to evaluate the adequacy of the SEM for improving the SSO stability by optimizing PMSG parameters, it is necessary to analyze the damping coupling characteristics between the two SSO modes with the change of PMSG parameters.

It can be seen from Table V that the two SSO modes are mainly affected by the DC voltage controllers in the GSCs of the wind farms, and the MSC controllers have a negligible impact on the two SSO modes. Therefore, the impact of the DC voltage controller, the filter inductance and the DC capacitance of PMSGs on the damping coupling characteristics should be analyzed.

Based on the two-generator small-signal model of (3) and the parameters in [43], as the DC voltage controller parameters, the filter inductor and the DC capacitor increase (the parameters of two PMSGs are changed at the same time), the trends of the two SSO eigenvalues are shown in Fig. 9. Accordingly, the damping trends of the two SSO modes are obtained, as shown in Table VI.

Table VI shows that with the change of PMSG parameters, the damping of the SSO_1 mode and SSO_2 mode increases or decreases simultaneously. Therefore, while optimizing PMSG parameters to suppress the SSO_2 in the SEM, the SSO_1 that is produced by the interactions among PMSGs in practical projects can be suppressed. This conclusion implies that the SEM is suitable for improving the SSO stability of the multi-machine system by optimizing the PMSG parameters.

This article has been accepted for publication in a future issue of this journal, but has not been fully edited. Content may change prior to final publication. Citation information: DOI 10.1109/TEC.2020.3028546, IEEE Transactions on Energy Conversion

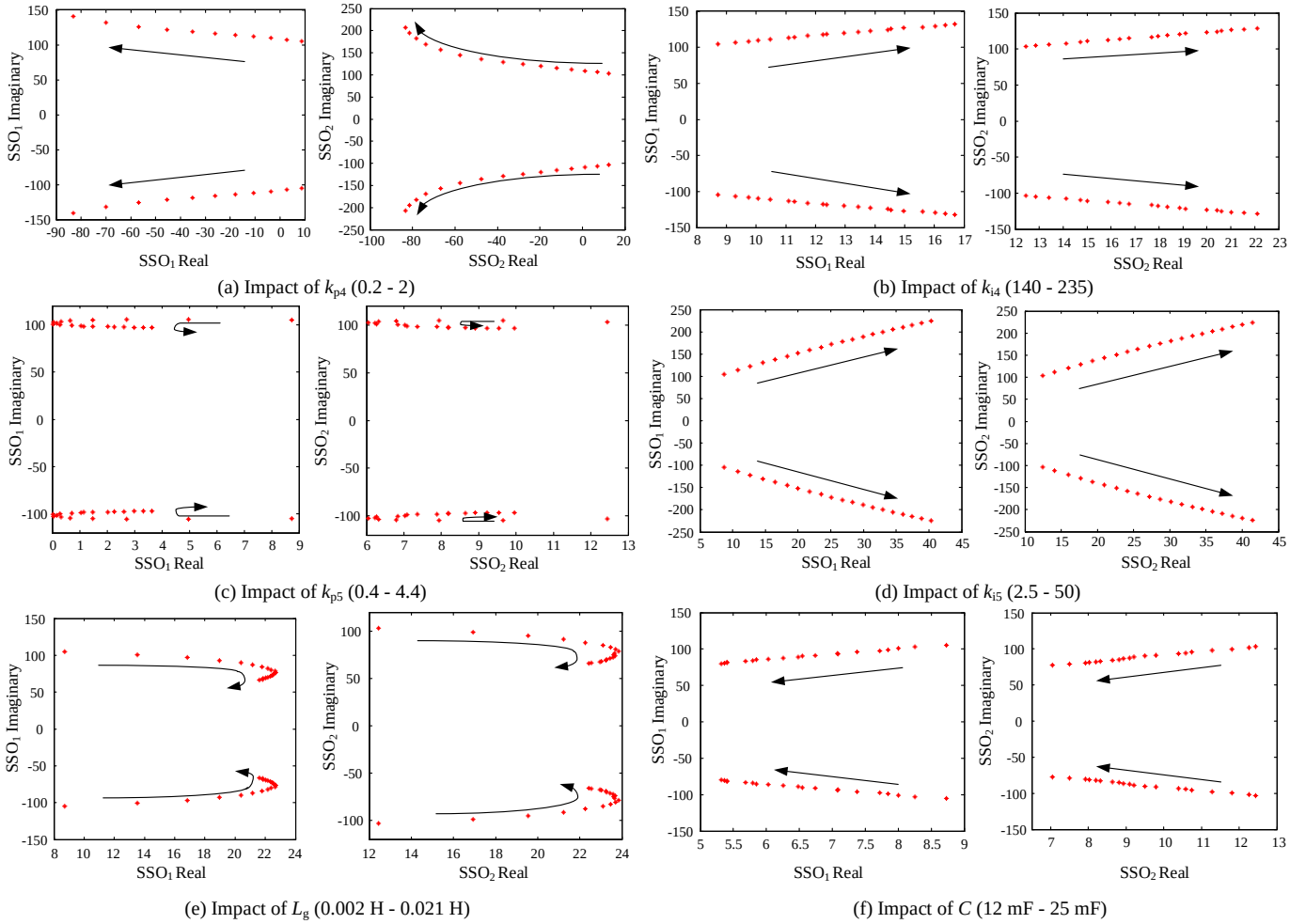

(a) Impact of k_{p4} (0.2 - 2) (b) Impact of k_{i4} (140 - 235)

(c) Impact of k_{p5} (0.4 - 4.4) (d) Impact of k_{i5} (2.5 - 50)

(e) Impact of L_g (0.002 H - 0.021 H) (f) Impact of C (12 mF - 25 mF)

Fig. 9. Impact of PMSG parameters on two coupling SSO modes in a two-generator PMSG-based wind farm with the VSC-HVDC: k_{p4} - outer loop proportional coefficient, k_{i4} - outer loop integral coefficient, k_{p5} - inner loop proportional coefficient, k_{i5} - inner loop integral coefficient, L_g - filter inductor, C - DC capacitor.

TABLE VI
THE IMPACT OF PMSG PARAMETERS ON THE DAMPING CHARACTERISTICS OF TWO SSO MODES

Parameters	Damping of SSO_1	Damping of SSO_2
Outer loop proportional coefficient k_{p4} ↑	↑	↑
Outer loop integral coefficient k_{i4} ↑	↓	↓
Inner loop proportional coefficient k_{p5} ↑	↑-↓	↑-↓
Inner loop integral coefficient k_{i5} ↑	↓	↓
Filter inductor L_g ↑	↓-↑	↓-↑
DC capacitor C ↑	↑	↑

Note: ↑ denotes increase; ↓ denotes decrease; ↑-↓ denotes increase first and then decrease; ↓-↑ denotes decrease first and then increase.

In order to verify the theoretical analysis, k_{i4} is changed from 20 to 200 and 400 at 1.5 s, respectively. Based on the PSCAD/EMTDC simulation model of a two-generator system in Fig. 3, the responses of the output active power P_1, P_2 in the first and second PMSGs and the output active power P_v in the VSC-HVDC are shown in Fig. 10. Fig. 10(a) shows that the output active power in the wind farm diverges with time gradually, and the damping when k_{i4} = 400 is smaller than the damping when k_{i4} = 200. Similarly, the same conclusion can be drawn in the output active power of the VSC-HVDC from Fig. 10(b). Therefore, with the increase of k_{i4}, the damping of the SSO_1 mode and SSO_2 mode reduces simultaneously, which verifies the theoretical analysis shown in Table VI.

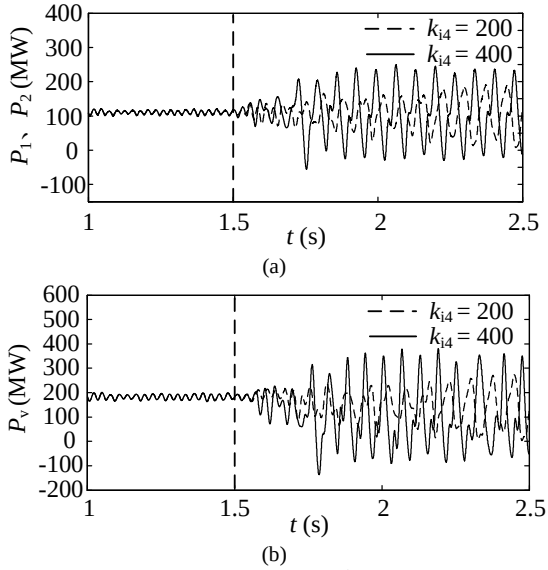

Fig. 10. Simulation results when k_{i4} changes from 20 to 200 and 400 in the two-generator system: (a) output active power P_1 and P_2 in PMSGs and (b) output active power P_v of the VSC-HVDC.

V. Conclusion

In this paper, the dynamic models of a two-generator system and the SEM of the DDWFV were built. Through the eigenvalue analysis and participation factors analysis, a stability comparison between the TEM and the SEM was presented, and the time-domain simulations were further performed to verify the theoretical analysis. The adequacy of the SEM for stability analysis in the DDWFV is explored in two aspects, which are summarized as follows:

From the perspective of the adequacy for oscillation modes analysis, the SEM preserves the dynamic characteristics of the wind-farm-grid SSO modes and the frequency characteristics of the TEM, but there are differences in the number of modes and their damping. The SEM and the TEM both contain wind-farm-grid SSO modes that are mainly affected by the grid-side DC voltage controllers in PMSGs and the *d*-axis voltage controller of the rectifier in the VSC-HVDC. However, compared with the TEM, the SEM contains more wind-farm-grid medium-frequency modes. These modes are merely the result of aggregation. Meanwhile, the TEM contains more inside-wind-farm SSO modes compared with the SEM, which are mainly affected by the grid-side DC voltage controllers in PMSGs. Moreover, there is a significant difference in the damping of certain medium-frequency modes between the SEM and the TEM. Therefore, the single-generator aggregation of wind farm hides some of the internal oscillation modes (e.g., unstable inside-wind-farm SSO modes) within wind farms or alter their characteristics, and certain additional medium-frequency modes exist because of the aggregation of cable parameters. An improved aggregation method should be developed as future work to preserve the critical modes of the DDWFV without adding other modes.

On the other hand, from the perspective of the adequacy for improving the SSO stability by optimizing the PMSG parameters, the SEM is suitable because the damping trends of inside-wind-farm SSO_1 modes and wind-farm-grid SSO_2 modes are identical with the change of the PMSG parameters. By optimizing the PMSG parameters to suppress the SSO_2 in the SEM, the SSO_1 that is produced by the interactions among PMSGs in practical projects is suppressed.

This paper only presents the adequacy analysis of the SEM compared with the WTGs in parallel connection. The future studies will focus on the improved single-generator aggregation method and the adequacy analysis of the SEM compared with the groups of WTGs in other connections.

References

[1] A. B. Mogstad, M. Molinas, P. K. Olsen, and R. Nilsen, "A power conversion system for offshore wind parks," in *Proc. IECON*, 2008, pp. 2106-2112.

[2] R. Basak, G. Bhuvaneswari, and R. R. Pillai, "Low-voltage ride-through of a synchronous generator-based variable speed grid-interfaced wind energy conversion system," *IEEE Trans. Ind. Appl.*, vol. 56, no. 1, pp. 752-762, Jan.-Feb. 2020.

[3] M. Amin and M. Molinas, "Understanding the origin of oscillatoryphenomena observed between wind farms and HVdc Systems," *IEEE J. Emerg. Sel. Top. Power Electron.*, vol. 5, no. 1, pp. 378-392, Mar. 2017.

[4] J. Lv, P. Dong, G. Shi, X. Cai, H. Rao, and J. Chen, "Subsynchronous oscillation of large DFIG-based wind farms integration through MMC-based HVDC," in *Proc. 2014 International Conference on Power System Technology*, 2014, pp. 2401-2408.

[5] C. Buchhagen, C. Rauscher, A. Menze, and J. Jung, "BorWin1 - First experiences with harmonic interactions in converter dominated grids," in *Proc. International ETG Congress 2015; Die Energiewende - Blueprints for the new energy age*, 2015, pp. 1-7.

[6] A. M. S. Al-bayati, F. Mancilla-David, and J. L. Dominguez-Garcial, "Aggregated models of wind farms: current methods and future trends," in *Proc. NAPS*, Denver, CO, 2016, pp. 1–6.

[7] M. J. Mercado-Vargas, D. Gomez-Lorente, O. Rabaza, and E. Alameda-Hernandez, "Aggregated models of permanent magnet synchronous generators wind farms," *Renew. Energy*, vol. 83, pp. 1287-1298, Nov. 2015.

[8] H. R. Ali, L. P. Kunjumuhammed, B. C. Pal, A. G. Adamczyk, and K. Vershinin, "Model order reduction of wind farms: linear approach," *IEEE Trans. Sustain. Energy*, vol. 10, no. 3, pp. 1194-1205, Jul. 2019.

[9] I. Al-ledani and Z. Gajic, "Order reduction of a wind turbine energy system via the methods of system balancing and singular perturbations," *Int. J. Electr. Power Energy Syst.*, vol. 117, pp. 105642, May 2020.

[10] D. Kim and M. A. El-Sharkawi, "Dynamic equivalent model of wind power plant using an aggregation technique," *IEEE Trans. Energy Convers.*, vol. 30, no. 4, pp. 1639-1649, Dec. 2015.

[11] H. R. Ali, L. P. Kunjumuhammed, B. C. Pal, A. G. Adamczyk, and K. Vershinin, "A trajectory piecewise-linear approach to nonlinear model order reduction of wind farms," *IEEE Trans. Sustain. Energy*, vol. 11, no. 2, pp. 894-905, Apr. 2020.

[12] W. Du, W. Dong, H. Wang, and J. Cao, "Dynamic aggregation of same wind turbine generators in parallel connection for studying oscillation stability of a wind farm," *IEEE Trans. Power Syst.*, vol. 34, no. 6, pp. 4694-4705, Nov. 2019.

[13] W. Du, W. Dong, and H. Wang, "A method of reduced-order modal computation for planning grid connection of a large-scale wind farm," *IEEE Trans. Sustain. Energy*, vol. 11, no. 3, pp. 1185-1198, Jul. 2020.

[14] J. Brochu, C. Larose, and R. Gagnon, "Validation of single- and multiple-machine equivalents for modeling wind power plants," *IEEE Trans. Energy Convers.*, vol. 26, no. 2, pp. 532-541, Jun. 2011.

[15] J. Lyu, X. Cai, and M. Molinas, "Frequency domain stability analysis of MMC-based HVdc for wind farm integration," *IEEE J. Emerg. Sel. Top. Power Electron.*, vol. 4, no. 1, pp. 141-151, Mar. 2016.

[16] J. Lyu and X. Cai, "Impact of controller parameters on stability of MMC-based HVDC systems for offshore wind farms," in *Proc. International Conference on Renewable Power Generation (RPG 2015)*, 2015, pp. 1-6.

[17] J. Lyu, X. Cai, and M. Molinas, "Optimal design of controller parameters for improving the stability of MMC-HVDC for wind fram integration," *IEEE J. Emerg. Sel. Top. Power Electron.*, vol. 6, no. 1, pp. 40-53, Mar. 2018.

[18] J. Lyu, M. Molinas, and X. Cai, "Stabilization control methods for enhancing the stability of wind farm integration via an MMC-based HVDC," in *Proc. CPE-POWERENG*, 2017, pp. 324-329.

[19] J. Lyu, X. Cai, M. Amin, and M. Molinas, "Sub-synchronous oscillation mechanism and its suppression in MMC-based HVDC connected wind farms," *IET Gener. Transm. Distrib.*, vol. 12, no. 4, pp. 1021-1029, Feb. 2018.

[20] W. Li, P. Chao, X. Liang, D. Xu, and X. Jin, "An improved single-machine equivalent method of wind power plants by calibrating power recovery behaviors," *IEEE Trans. Power Syst.*, vol. 33, no. 4, pp. 4371-4381, Jul. 2018.

[21] Y. Wang, C. Lu, L. Zhu, G. Zhang, X. Li, and Y. Chen, "Comprehensive modeling and parameter identification of wind farms based on wide-area measurement systems," *J. Mod. Power Syst. Clean Energy*, vol. 4, no. 3, pp. 383-393, Jul. 2016.

[22] H. Li, C. Yang, B. Zhao, H. S. Wang, and Z. Chen, "Aggregated models and transient performances of a mixed wind farm with different wind turbine generator systems," *Elect. Power Syst. Res.*, vol. 92, pp. 1-10, Nov. 2012.

[23] L. P. Kunjumuhammed, B. C. Pal, R. Gupta, and K. J. Dyke, "Stability analysis of a PMSG-based large offshore wind farm connected to a VSC-HVDC," *IEEE Trans. Energy Convers.*, vol. 32, no. 3, pp. 1166-1176, Sept. 2017.

[24] M. Y. Morgan, A. A. EI-Deib, and M. EI-Marsafawy, "Wind farm dynamic models assessment under weak grid conditions," *IET Renew. Power Gener.*, vol. 12, no. 12, pp. 1325-1334, Sept. 2018.

[25] G. Tapia, A. Tapia, and J. X. Ostolaza, "Two alternative modeling approaches for the evaluation of wind farm active and reactive power performances," *IEEE Trans. Energy Convers.*, vol. 21, no. 4, pp. 909–920,

Dec. 2006.

[26] V. Akhmatov and H. Knudsen, "An aggregate model of a grid-connected, large-scale, offshore wind farm for power stability investigations: Importance of windmill mechanical system," *Int. J. Elect. Power Energy Syst*., vol. 24, no. 9, pp. 709–717, Nov. 2002.

[27] A. Perdana and C. Ola, "Aggregated models of a large wind farm consisting of variable speed wind turbines for power system stability studies," in *Proc. 8th Int. Workshop Large-Scale Integr. Wind Power Power Syst. Well Transmiss. Netw. Offshore Wind Farms*, pp. 568–573, 2009.

[28] B. Huang, H. Sun, Y. Liu, L. Wang, and Y. Chen, "Study on subsynchronous oscillation in D-PMSGs-based wind farm integrated to power system," *IET Renew. Power Gener.*, vol. 13, no. 1, pp. 16-26, Jan. 2019.

[29] Y. Wu, J. Zeng, G. Lu, S. Chau, and Y. Chiang, "Development of an equivalent wind farm model for frequency regulation," *IEEE Trans. Ind. Appl*., vol. 56, no. 3, pp. 2360-2374, May-Jun. 2020.

[30] J. Ruan, Z. Lu, Y. Qiao, and Y. Min, "Analysis on applicability problems of the aggregation-based representation of wind farms considering DFIGs' LVRT behaviors," *IEEE Trans. Power Syst*., vol. 31, no. 6, pp. 4953-4965, Nov. 2017.

[31] E. Muljadi and B. Parsons, "Comparing single and multiple turbine representations in a wind farm simulation," *Eur. Wind Energy Conf.*, Athens, Greece, Jan. 2006, pp. 1-10.

[32] X. He, H. Geng, G. Yang, X. Zou, and Y. Li, "Equivalent modelling of wind farm for small-signal stability analysis in weak power system," *The Journal of Engineering* vol. 2017, no. 13, pp. 1388-1393, 2017.

[33] Y. Zhou, L. Zhao, and W. Lee, "Robustness analysis of dynamic equivalent model of DFIG wind farm for stability study," *IEEE Trans. Ind. Appl*., vol. 54, no. 6, pp. 5682-5690, Nov.-Dec. 2018.

[34] Y. Zhou, L. Zhao, T. Hsieh, and W. Lee, "A multistage dynamic equivalent modeling of a wind farm for the smart grid development," *IEEE Trans. Ind. Appl*., vol. 55, no. 5, pp. 4451-4461, Sept.-Oct. 2019.

[35] D. Kim and M. A. El-Sharkawi, "Dynamic equivalent model of wind power plant using parameter identification," *IEEE Trans. Energy Convers.*, vol. 31, no. 1, pp. 37-45, Mar. 2016.

[36] J. Ma, F. Liu, L. Jiang, M. Wu, Y. Li, and W. Wang, "Multi-DFIG aggregated based SSR analysis considering wind spatial distribution," *IET Renew. Power Gener*., vol. 13, no. 4, pp. 549-554, Mar. 2019.

[37] H. Liu, X. Xie, X. Gao, H. Liu, and Y. Li, "Stability analysis of SSR in multiple wind farms connected to series-compensated systems using impedance network model," *IEEE Trans. Power Syst.*, vol. 33, no. 3, pp. 3118-3128, May 2018.

[38] S. Liao. X. Zha, X. Li, M. Huang, J. Sun, J. Pan, and J. M. Guerrero, "A novel dynamic aggregation modeling method of grid-connected inverters: application in small-signal analysis," *IEEE Trans. Sustain. Energy*, vol. 10, no. 3, pp. 1554-1564, Jul. 2019.

[39] X. Zha, S. Liao, M. Huang, Z. Yang, and J. Sun, "Dynamic aggregation modeling of grid-connected inverters using Hamilton's-action-based coherent equivalence," *IEEE Trans. Ind. Electron.*, vol. 66, no. 8, pp. 6437-6448, Aug. 2019.

[40] L. P. Kunjumuhammed, B. C. Pal, C. Oates, and K. J. Dyke, "The adequacy of the present practice in dynamic aggregated modeling of wind farm systems," *IEEE Trans. Sustain. Energy*, vol. 8, no. 1, pp. 23-32, Jan. 2017.

[41] L. P. Kunjumuhammed, B. C. Pal, C. Oates, and K. J. Dyke, "Electrical oscillations in wind farm systems: analysis and insight based on detailed modelling," *IEEE Trans. Sustain. Energy*, vol. 7, no. 1, pp. 51-62, Jan. 2014.

[42] H. Huang. C. Mao, J. Lu, and D. Wang, "Small-signal modelling and analysis of wind turbine with direct drive permanent magnet synchronous generator connected to power grid," *IET Renew. Power Gener*., vol. 6, no. 1, pp. 48-58, Jan. 2012.

[43] S. Zhao and B. Shao, "An analytical method suitable for revealing the instability mechanism of power electronics dominated power systems," *Int. J. Electr. Power Energy Syst*., vol. 109, pp. 269-282, Jul. 2019.

[44] J. Z. Zhou, H. Ding, S. Fan, Y. Zhang, and A. M. Gole, "Impact of short-circuit ratio and phase-locked-loop parameters on the small-signal behavior of a VSC-HVDC converter," *IEEE Trans. Power Deliv.*, vol. 29, no. 5, pp. 2287-2296, Oct. 2014.

[45] E. Muljadi, S. Pasupulati, A. Ellis, and D. Kosterov, "Method of equivalencing for a large wind power plant with multiple turbine representation," in *Proc. Power Energy Soc. General Meeting—Convers. Delivery Elect. Energy 21st Century*, Pittsburgh, PA, 2008, pp. 1–9.

[46] L. M. Fernandez, C. A. Garcia, J. R. Saenz, and F. Jurado, "Reduced model of DFIGs wind farms using aggregation of wind turbines and the equivalent wind," in *Proc. Mediterranean Electrotechnical*, Malaga, 2006, pp. 881–884.

[47] H. Liu and J. Sun, "Voltage stability and control of offshore wind farms with AC collection and HVDC transmission," *IEEE J. Emerg. Sel. Top. Power Electron*., vol. 2, no. 4, pp. 1181-1189, Dec. 2014.

[48] Y. Zhang, E. Muljadi, D. Kosterev, and M. Singh, "Wind power plant model validation using synchrophasor measurements at the points of interconnection," *Trans. Sustain. Energy*, vol. 6, no. 3, pp. 984-992, Jul. 2015.

[49] G. Li, W. Wang, C. Liu, Y. Jin, and G. He, "Mechanism analysis and suppression method of wideband oscillation of PMSG wind farms connected to weak grid (Part I): analysis of wideband impedance characteristics and oscillation mechanism," *Proc. CSEE*, vol. 39, no. 22, pp. 6547-6562, Nov. 2019.